Mon. Not. R. Astron. Soc. **000**, 000–000 (0000) Printed 27 January 2014 (MN LATEX style file v2.2)

Orbital motion effects in astrometric microlensing

Sedighe Sajadian ⋆
School of Astronomy, IPM (Institute for Research in Fundamental Sciences), P.O. Box 19395-5531, Tehran, Iran

arXiv:1401.6416v1 [astro-ph.IM] 24 Jan 2014

27 January 2014

ABSTRACT
We investigate lens orbital motion in astrometric microlensing and its detectability. In microlensing events, the light centroid shift in the source trajectory (the astrometric trajectory) falls off much more slowly than the light amplification as the source distance from the lens position increases. As a result, perturbations developed with time such as lens orbital motion can make considerable deviations in astrometric trajectories. The rotation of the source trajectory due to lens orbital motion produces a more detectable astrometric deviation because the astrometric cross-section is much larger than the photometric one. Among binary microlensing events with detectable astrometric trajectories, those with stellar-mass black holes have most likely detectable astrometric signatures of orbital motion. Detecting lens orbital motion in their astrometric trajectories helps to discover further secondary components around the primary even without any photometric binarity signature as well as resolve close/wide degeneracy. For these binary microlensing events, we evaluate the efficiency of detecting orbital motion in astrometric trajectories and photometric light curves by performing Monte Carlo simulation. We conclude that astrometric efficiency is 87.3 per cent whereas the photometric efficiency is 48.2 per cent.

1 INTRODUCTION

Gravitational field of an object acts as a gravitational lens which deviates light path of a collinear background source and produces distorted images (Einstein 1936). In Galactic scale, the angular separation of the images is of order of milli-acrsecond that is too small to be resolved even by the most modern telescopes. Instead, the combined light of images received by an observer is magnified in comparison to the un-lensed source. This phenomenon is called gravitational microlensing which was proposed as a method to probe dark objects in Galactic halo, extra solar planets, study stellar atmosphere, etc.(Liebes 1964; Chang & Refsdal 1979; Paczyński 1986a,b).

One of features of gravitational microlensing is the deviation of the light centroid of the source star images from the source star position. For the case of a point-mass lens, the centroid shift of source star images traces an ellipse in the lens plane while the source star is passing an straightforward line in the lens plane (Walker 1995; Miyamoto & Yoshii 1995; Høg et al. 1995; Jeong et al. 1999). In contrast with the magnification factor which is a dimensionless scalar, the light centroid shift of the source star images is a dimensional vector and its size is proportional to angular Einstein radius, i.e. the angular radius of images ring when observer, source and lens are completely aligned. For a stellar-mass lens, the angular Einstein radius is a few hundreds micro-arcsecond, too small to be observed directly. However, its quantity enhances in two cases: (i) when the lens mass is high, e.g. a stellar-mass black hole as microlens and (ii) when the lens is very close to the observer. The light centroid shift of source star images in these microlensing events is measurable by high-precision interferometers e.g. Very Large Telescope Interferometry (VLTI) or the HST (Paczyński 1995). An important future project is GAIA, performing high precision astrometry, which will be operational in near future (Proft et al. 2011).

During a microlensing event by measuring the astrometric lensing and parallax effects, the mass of the deflector can be inferred without knowing the exact distances of the lens and the source from the observer (Paczyński 1997; Miralda-Escdé 1996). Also the degeneracy in close/wide caustic-crossing binary microlensing events (Dominik 1999) can be removed by astrometric measurements (Gould & Han 2000; Chung et al. 2009). The two configurations of the lens and source produce different astrometric trajectories even though they might present the same light curves. Hence, by measuring the astrometric trajectories this degeneracy can be removed (Han et al. 1999).

Generally, there are some anomalies in microlensing events which deviate the observed light curve and astrometric trajectory of source star from the standard model. Some deviations owing to these anomalies help obtain extra information about lens and source and thus resolve degeneracy. One of them is the effect of lens orbital motion in a binary microlensing event. In this case two components in a gravitationally bound binary system which act as lens rotate around their common center of mass. As a result, their orientation changes as a microlensing event progress and the resulting light curve is different from that due to a static binary microlens. The ratio of the Einstein crossing time to the orbital period of lens system is considered as a criterion which indicates the probability of detecting the orbital motion in the microlensing light curve (Dominik 1998; Ioka et al. 1999). Measuring this effect gives information about the orbit of microlenses system which in turn helps to resolve the close/wide degeneracy (An et al. 2002; Gaudi et al. 2008; Dong et al. 2009; Shin et al. 2013). Detectability of orbital motion in light curves of binary microlensing events was investigated extensively by Penny et al. (2011) whereas the rel-

© 0000 RAS

evant deviation in the astrometric trajectory of source star and its detectability are not clear yet.

In this work, we study lens orbital motion in astrometric microlensing and its detectability. In microlensing events, the astrometric trajectory of source star tends to zero much more slowly than the light amplification as the source distance from the lens position rises. As a result, perturbations enlarged with time such as lens orbital motion can produce considerable deviations in the astrometric trajectories. Since the astrometric cross-section is much larger than the photometric one, so the rotation in the source trajectory owing to the orbital motion is more probable to be detected in the astrometric trajectory than the photometric light curve. However, depending on the size of the angular Einstein radius this effect can be detected. We find that, among binary microlensing events with detectable astrometric trajectories, those with rotating stellar-mass black holes have most likely detectable astrometric signatures of orbital motion. For these binary microlensing events, we evaluate the efficiency of detecting orbital motion in astrometric trajectories and photometric light curves by performing Monte Carlo simulation. Detecting lens orbital motion in their astrometric trajectories helps to discover even secondary components with no photometric binarity signatures as well as resolve close/wide degeneracy.

This paper is organized as follows: In section (2) the effect of orbital motion in binary microlensing events are explained. We next describe astrometric properties of microlensing events and finally we investigate the orbital motion effect on the astrometric trajectories. In the next section by preforming a Monte Carlo simulation we study the astrometric and photometric efficiencies for detecting lens orbital motion. In section (4) we explain the results.

2 ORBITAL MOTION IN ASTROMETRIC MICROLENSING

In this section we first study the orbital motion effect in binary microlensing events. Having reviewed the astrometric microlensing, we investigate the microlensing events with detectable astrometric shifts in source trajectories. Finally, we study whether the orbital motion effect in the astrometric trajectories is detectable.

2.1 Orbital motion effect of binary microlenes

Dominik (1998) first studied the effect of lens orbital motion in binary microlensing events and concluded that in the most microlensing events this effect is ignorable, but in some long-duration microlensing events can probably be observed. Orbital motion effects on the planetary signals in high-magnification microlensing events was investigated by Rattenbury et al. (2002). Recently, Penny et al. (2012) indicated how fraction of binary and planetary microlensing events exhibit the orbital motion effects in their light curves by performing Monte Carlo simulation and investigated those factors which change this fraction. Until now, several observed microlensing events have shown the signatures of lens orbital motion. In some cases, these signatures have allowed to infer some of orbital parameters and remove the close/wide degeneracy (An et al. 2002; Gaudi et al. 2008; Dong et al. 2009; Shin et al. 2013). Sometimes, there are several degenerate best-fitting solutions for orbital motion modeling. Three systems with complete orbital solutions have been found, e.g. the microlensing event OGLE-2011-BLG-0417 (Shin et al. 2011; Shin et al. 2012). However, one of these solutions can actually be checked with radial velocity method (Gould et al. 2013). In the following we study the orbital motion effect in microlensing light curves in the same way as Dominik's approach.

Let us consider a gravitationally bound system as microlens. Under the gravitational effect, the secondary component with respect to the first one traces out an ellipse one of whose focus is at the center of mass position. Two components of their relative distance are given by:

$$\begin{aligned} x(\xi) &= a(\cos\xi - \varepsilon) \\ y(\xi) &= a\sqrt{1-\varepsilon^2}\sin\xi, \end{aligned} \quad (1)$$

where x and y axes are along the semi-major and semi-minor axes, ε is the eccentricity, a is the semi-major axis and ξ is a periodic function with time which for a small eccentricity and up to its first order is estimated as:

$$\xi(t) = 2\pi\frac{t-t_p}{P} + 2\varepsilon\sin(2\pi\frac{t-t_p}{P}), \quad (2)$$

where t_p is the time of arriving at the perihelion point of orbit, P is the orbital period of the lenses motion. To study the orbital motion of lenses on microlensing light curves, we should project the orbit plane of lenses into the sky plane. In that case, we need to two consecutive rotation angles: β around x-axis and γ around y-axis. The projected components of the relative position vector of the second one with respect to the first, in the sky plane normalized to the Einstein radius are:

$$\begin{aligned} x_1(t) &= \rho[\cos\gamma(\cos\xi(t)-\varepsilon) + \\ &\quad + \sin\beta\sin\gamma\sqrt{1-\varepsilon^2}\sin\xi(t)] \\ x_2(t) &= \rho\cos\beta\sqrt{1-\varepsilon^2}\sin\xi(t), \end{aligned} \quad (3)$$

where ρ is the normalized semi-major axis to the Einstein radius (Dominik 1998). Hence, lens orbital motion causes the projected distance between two lenses in the lens plane changes with time which is given by:

$$d(t) = \sqrt{x_1(t)^2 + x_2(t)^2}. \quad (4)$$

On the other hand, the binary axis with respect to the projected source trajectory rotates with angle $\theta_l(t) = \tan^{-1}(x_2/x_1)$. So, during a microlensing event with binary rotating lenses, the source trajectory rotates with respect to the binary axis with angle $-\theta_l$ around the line of sight towards the observer. However, this rotation is not always detectable in the observer reference frame.

The signature of lens orbital motion in the microlensing light curves is not always observable and its Detectability depends strongly on the ratio of the lensing characteristic time to the orbital period of lenses motion. Dominik (1998) considered the Einstein crossing time as the characteristic time of a binary microlensing event to evaluate the orbital motion detectability. However, the orbital motion detection efficiency for binary microlensing events without caustic-crossing features is too small and of order of one per cent (Penny et al. 2011). As a result, we consider the effective time scale for detecting signatures of lens orbital motion as $\tilde{t_E} = \Delta(q,d)t_E$ instead of the Einstein crossing time, where $\Delta(q,d)$ refers to the average over the ratios of the lengths of the source trajectories providing the sources are inside the caustic curve to the total length of the source trajectories. We assume that there are several parallel source trajectories over the lens plane with the same lengths i.e. L so that they cover the caustic curve. In this case, $\Delta(q,d)$ is given by:

$$\Delta(q,d) = \frac{1}{L}(\sum_i^N l_i/N) = \frac{1}{NL\delta}\sum_i^N l_i\delta = \mathcal{S}_c, \quad (5)$$

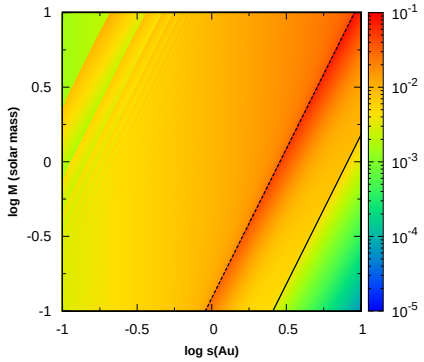

Figure 1. The map of the detectability factor f in the lenses parameter space containing the lenses total mass M and the semi-major axis of lenses orbit s. The black dashed and solid lines represent the branch values of the projected distance between two lenses normalized to the Einstein radius between 3 different topologies of caustic: close, intermediate and wide binaries respectively.

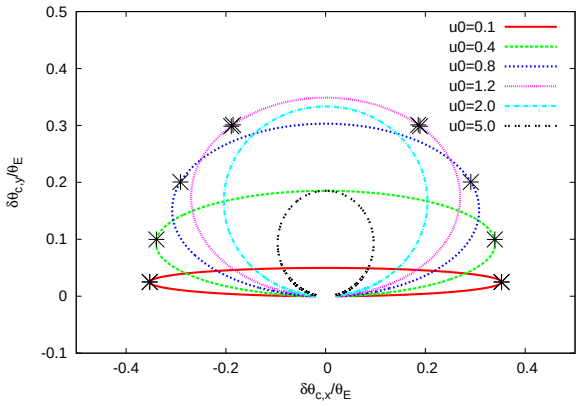

Figure 2. The trajectory of the light centroid shift normalized to the θ_E assuming a point-like source star is passing an straightforward line in the gravitational field of a point-mass lens for various amounts of impact parameter. The star signs indicate the most deviation in the light centroid of images with respect to the source position which happens at $u = \sqrt{2}$.

where l_i is the length of the portion of ith source trajectory providing the source is inside the caustic curve, N is the number of the source trajectories, $\delta = L/N$ is the normal distance between two consecutive source trajectories, d is the projected distance between two lenses normalized to the Einstein radius and q is the ratio of the lens masses. According to equation (5), it is clear that $\Delta(q, d)$ is equal to the ratio of the area interior to the caustic curve to an area equal to L^2 i.e. $\mathcal{S}_c$. By considering this factor, the detectability of lens orbital motion can be characterized by the factor f:

$$f = \frac{\tilde{t_E}}{P}. \tag{6}$$

The map of detectability factor f is shown in Figure (1) in the parameter space of lenses containing the total mass of lenses M and semi-major axis s. In this figure the black dashed and solid lines represent the threshold values between the close-intermediate (or resonance) and intermediate-wide binaries respectively. For calculating the inner area of caustics, we first determine the caustic points which have so small determinant of Jacobian matrix. Then, after sorting the consecutive points on the caustic line we calculate the interior area of caustics numerically. The detectability factor has the highest amount for the intermediate microlensing events which locate near to the close-intermediate threshold line (dashed line). However, Gaudi (2012) intuitively pointed out that the resonance microlensing events according to their large sizes and cross-sections are more sensitive to the small changes in d owing to lens orbital motion. According to this figure, the orbital motion detectability in microlensing events with more massive lenses which have the same caustic curve, is larger than those with less massive lenses. For this plot, we consider $q = 1$, $v_t = 175km/s$, $D_l = 4Kpc$ and $D_s = 8Kpc$. However, the smaller amounts of q just move two threshold lines towards each other so that they mostly form close and wide binaries while the detectability factor is maximum for intermediate binaries similar to the plotted case.

In the following, we explain the astrometric properties of microlensing and seek binary microlensing events which have detectable astrometric trajectories as well as very likely detectable orbital motion signatures.

2.2 Astrometric properties of microlensing

In microlensing events, the light centroid vector of source star images does not coincide with the source position. This astrometric shift in source star position changes with time as a microlensing event progresses. For a point-mass lens, the centroid shift vector of source star images is given by:

$$\boldsymbol{\delta\theta}_c = \frac{\mu_1\boldsymbol{\theta_1} + \mu_2\boldsymbol{\theta_2}}{\mu_1 + \mu_2} - \boldsymbol{u}\theta_E = \frac{\theta_E}{u^2+2}\boldsymbol{u}, \tag{7}$$

where $\boldsymbol{\theta}_i$ and μ_i are the position and magnification factor of ith image, $\boldsymbol{u} = p\hat{x} + u_0\hat{y}$ is the vector of the projected angular position of the source star with respect to the lens normalized by the angular Einstein radius of the lens θ_E in which $p = (t - t_0)/t_E$, t_0 is the time of the closest approach, t_E is the Einstein crossing time, $\hat{x}$ and $\hat{y}$ are the unit vectors in the directions parallel with and normal to the direction of the lens-source transverse motion. The angular Einstein radius of lens is given by:

$$\theta_E = \sqrt{\kappa\, M_l\, \pi_{rel}} = 300\mu as\sqrt{\frac{M_l}{0.3M_\odot}}\sqrt{\frac{\pi_{rel}(mas)}{0.036}}, \tag{8}$$

where M_l is the lens mass, $\kappa = \frac{4G}{c^2 Au}$ and $\pi_{rel} = 1Au(\frac{1}{D_l} - \frac{1}{D_s})$ where D_l and D_s are the lens and source distances from the observer. Usually, a microlensing parallax is defined as $\pi_E = \pi_{rel}/\theta_E$ which can be measured from the photometric event.

The components of this centroid shift vector are given by:

$$\begin{aligned} \delta\theta_{c,x}(u_0, p) &= \frac{p}{u_0^2 + p^2 + 2}\theta_E, \\ \delta\theta_{c,y}(u_0, p) &= \frac{u_0}{u_0^2 + p^2 + 2}\theta_E. \end{aligned} \tag{9}$$

The shift in the light centroid trajectory of the source star images owing to a point-mass lens traces an ellipse while the source star is passing an straightforward line in the lens plane, plotted in Figure (2). By defining $X = \delta\theta_{c,x}$ and $Y = \delta\theta_{c,y} - \frac{u_0\theta_E}{2(u_0^2+2)}$, these coordinates satisfy the following equation:

$$X^2 + (\frac{Y}{b})^2 = a^2, \tag{10}$$

where $b = \frac{u_0}{\sqrt{u_0^2+2}}$ and $a = \frac{\theta_E}{2\sqrt{u_0^2+2}}$. This ellipse is called the *astrometric ellipse* (Walker 1995; Jeong et al. 1999). The ratio of the

	$M(M_\odot)$	$D_l(Kpc)$	$D_s(Kpc)$	$R_E(Au)$	$\theta_E(millias)$	$\mu_l(''/yr)$	$V_t(Km/s)$	$t_E(day)$	$s(Au)$	$P(day)$
$(\mathcal{A})$	$\geqslant 5$	~ 6.5	~ 8.0	$\geqslant 7.0$	$\geqslant 1.1$	~ 0.006	~ 175	$\geqslant 70$	~ 4	$\leqslant 1300$
$(\mathcal{B})$	~ 0.3	$\leqslant 0.1$	~ 8.0	$\leqslant 0.5$	$\geqslant 4.9$	$\geqslant 0.4$	~ 185	$\leqslant 5$	~ 4	~ 5000

Table 1. The possible ranges of physical parameters of two sets of binary microlensing events with measurable shifts in the astrometric light centroid of source star images: $(\mathcal{A})$ gravitational microlensing events with binary stellar-mass black holes and $(\mathcal{B})$ those with high proper motion stars located in distances smaller than 100 parsec from the sun.

axes of this ellipse is a function of impact parameter, so that for the large impact parameter this ellipse converts to a circle whose radius decreases by increasing impact parameter and for small amounts, it becomes a straight line (see Figure 2) (Walker 1995). since $\frac{a}{b} = \frac{2u_0}{\theta_E}$ and we can simply obtain u_0 from photometry, so from astrometric data we get the angular Einstein radius from which as well as the parallax measurement the lens mass can be inferred. In this figure the points with the maximum amounts of the centroid shift (i.e. $u = \sqrt{2}$) were shown with star symbols. For $u \gg \sqrt{2}$ the size of the astrometric centroid shift falls off as θ_E/u whereas the magnification factor of a point-like source star being lensed by a point-mass lens for $u \gg 1$ tends to $1 + 2/u^4$. Hence, the centroid shift of source star images falls off much more slowly than the light amplification of source while the source distance from the lens rises (Dominik & Sahu 2000). As a result, the astrometric cross-section is larger than the photometric one in microlensing events.

In contrast with the magnification factor which is a dimensionless scalar, the light centroid shift of the source star images is a dimensional vector and its size is proportional to the angular Einstein radius given by equation (8). The angular Einstein radius of a K- or M-dwarf star as the most probable lens with $M_l \sim 0.3M_\odot$ located in the Galactic disk $D_l \sim 6.5$Kpc, in the observations towards the Galactic bulge i.e. $D_s \sim 8.0$Kpc, is of order of a few hundred micro-arcsecond (see equation 8) which is too small to be observed. However, for two sets of microlensing events the angular Einstein radius enhances: $(\mathcal{A})$ when the lens mass is high and $(\mathcal{B})$ when the lens is so close to the observer. These two classes of microlensing events with detectable astrometric trajectories have different properties owing to different amounts of the Einstein radius. In table (1) we briefly express the possible ranges of amounts of their physical parameters.

The set $(\mathcal{A})$ of microlensing events which are characterized in the second row of table (1) are long-duration microlensing events with no light from the lens. These events with detectable astrometric trajectories are best candidates to indicate the mass of stellar-mass black holes located in the Galactic disk through the photometric and astrometric data as well as the parallax effect (Sahu 2011a). It has been five years since the HST started observing some of long-duration microlensing events with no light from the lens. Because no isolated black hole has been discovered to date, so these events very likely show binarity signatures (Sahu 2011b). The binary microlensing events due to stellar-mass black holes located in Galactic disk with the total mass of lenses larger than $5M_\odot$ and semi major axis of order of 4Au which have the orbital period larger than 1300days, are characterized by the Einstein radius larger than 7.8Au and the Einstein crossing time larger than 80days. Therefore, most of these events are close and a few of them are intermediate or wide binary microlensing events in which the orbital motion effect of lenses is not ignorable due to the considerable ratio of the Einstein crossing time to the orbital period and the finite size effect is too small owing to the large Einstein radius.

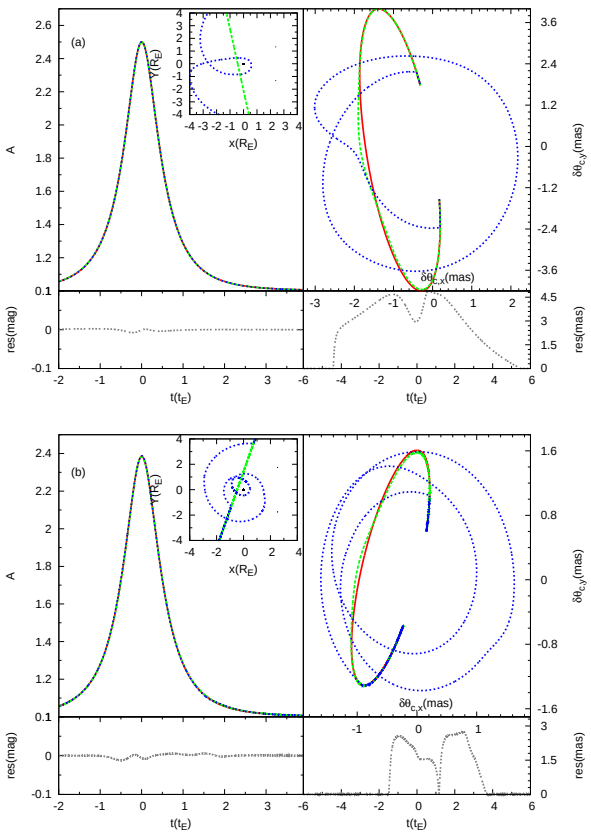

Figure 3. Two typical binary microlensing events with rotating stellar-mass black holes. In each subfigure, the light curves (left panels), astrometric trajectories (right panels) and the source trajectories with respect to the caustic curve (insets in the left-hand panels) without and with considering the effect of lens orbital motion are shown with green dashed and blue dotted lines respectively. The point-mass lens models are shown by red solid lines. The photometric and astrometric residuals with respect to the static binary model are plotted with gray dotted lines. The relevant parameters can be found in Table (2).

The second set $(\mathcal{B})$ which are characterized in the third row of table (1) contains gravitational microlensing events in which the lens is so close to the sun, e.g. closer than 100 parsec from the sun position. These stars are best candidates for the astrometric microlensing through GAIA mission for accurately indicating their mass(Proft et al. 2011). Owing to the small distance of the lens from the sun, their proper motion is so high and larger than 0.5 arcsecond in year. These microlensing events are characterized by the Einstein radius smaller than 0.5Au and Einstein crossing time smaller than 5days. Let us assume that the lens is a binary system. In that case, most of these binary microlensing events are wide and a few of them are intermediate or close microlensing events in

	$M_l(M_\odot)$	q	$s(Au)$	$d(R_E)$	$t_E(day)$	$P(day)$	β°	γ°	α°	u_0	$v_t(km/s)$
(a)	8.5	0.06	2.5	0.33	48.6	478.9	-5.3	85.7	101.7	0.43	271.6
(b)	13.7	0.09	3.9	0.28	276.7	734.8	-23.1	69.3	71.6	0.45	88.6
(c)	15.4	0.12	9.5	0.64	233.1	2572.1	40.3	-82.7	233.4	0.77	110.0

Table 2. The parameters used to make the microlensing light curves shown in Figure (3) and Figure (4).

which the orbital motion effect of lenses is ignorable due to the too small ratio of the Einstein crossing time to the orbital period and the finite-lens effect is probably considerable owing to the small Einstein radius. Note that, the finite-source effect is mostly ignorable because of the small amount of the relative distance of the lens to the source star from the observer i.e. $x(=D_l/D_s)\leqslant 0.0125$.

Hence, binary microlensing events with rotating stellar-mass black holes located in the Galactic disk which have detectable astrometric shifts in the source star trajectories have most likely detectable orbital motion signatures (case $\mathcal{A}$). In these events, the ratio of the Einstein crossing time to the orbital period is high. If there is no caustic-crossing feature in their light curves, the photometric signature of orbital motion or even of the secondary lens is too small to be detected whereas the astrometric signature owing to the orbital motion can be detected in the astrometric trajectories which can show the existence of a secondary component. In this work we pay attention to these events owing to much probability of detecting astrometric signatures of orbital motion.

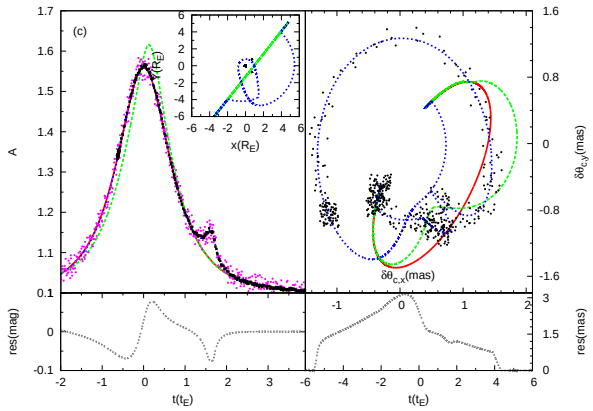

Figure 4. A simulated microlensing light curve and astrometric trajectory of source star. Data points taken by survey telescopes and the HST are shown with violet points and black stars. The parameters used to make this event can be found in table (2).

2.3 Astrometric microlensing with rotating stellar-mass black holes

Here, we study the astrometric microlensing due to rotating stellar-mass black holes. As mentioned, lens orbital motion changes the lenses orientation. As a result, the magnification pattern changes with time owing to the time variation of the projected distance between two lenses as well as the straightforward source trajectory rotates with respect to the binary axis. However, source star does not always receive the gravitational effect of the secondary component, e.g. when the ratio of the lens masses is so small. In that case, the source trajectory does not change in the observer reference frame. Considering this point, we let the lenses rotate around their common center of mass when the astrometric trajectory deviates more than 5 micro arcseconds from the astrometric ellipse due to a point-mass lens located at the center of mass position whose mass is equal to the total mass of the lenses. However, when this difference becomes smaller than the threshold amount, we stop the lenses rotation and let the source trajectory slowly return back to its straightforward trace.

In Figure (3) we represent two examples of microlensing events with rotating stellar-mass black holes. In each subfigure, the light curves (left panels) and astrometric trajectories (right panels) without and with considering the effect of lens orbital motion are shown with green dashed and blue dotted lines respectively. The point-mass lens models are shown by red solid lines. The photometric and astrometric residuals with respect to the static binary model are plotted with gray dotted lines. The parameters of these microlensing events can be found in Table (2). We use the generalized version of the adaptive contouring algorithm (Dominik 2007) for plotting astrometric trajectories in binary microlensing events. Even though, the orbital motion effect is not obvious in the light curves, this effect can be detected in the astrometric trajectories. The orbital motion of lenses makes the astrometric trajectory rotate in the same way as the source trajectory.

In the subfigure (b) some oscillatory fashions can be seen in the astrometric trajectory which is owing to lens orbital motion. Indeed, whenever the source trajectory does not cross the caustic curve, the astrometric centroid shift can be estimated as the case of point-mass lens, i.e. $\delta\theta'_c=\frac{u'}{u'^2+2}$ where $u'=\sqrt{x'^2_s+y'^2_s}$, x'_s and y'_s are the components of angular source-lens distance by considering the effect of lens orbital motion:

$$\begin{aligned}
x'_s &= \sqrt{1-\varepsilon^2}\sin\xi(t)[u_0(\cos\beta\cos\alpha-\sin\alpha\sin\beta\sin\gamma)\\
&+ p(t)(\cos\beta\sin\alpha+\sin\beta\sin\gamma\cos\alpha)]\\
&+ \cos\xi(t)\cos\gamma[p(t)\cos\alpha-u_0\sin\alpha]-p(t)\varepsilon\\
y'_s &= \sqrt{1-\varepsilon^2}\sin\xi(t)[u_0(\cos\beta\sin\alpha+\cos\alpha\sin\beta\sin\gamma)\\
&+ p(t)(-\cos\beta\cos\alpha+\sin\beta\sin\gamma\sin\alpha)]\\
&+ \cos\xi(t)\cos\gamma[u_0\cos\alpha+p(t)\sin\alpha]-u_0\varepsilon\cos\gamma, \quad (11)
\end{aligned}$$

where α is the angle between the source trajectory and the binary axis. By considering the orbital motion some oscillatory fashions, terms containing $\sin\xi$ and $\cos\xi$, will appear in the astrometric trajectories which depending on the ratio of the Einstein crossing time to the orbital period they or some parts of them can be detected.

When the angle between the orbital motion plane of lenses and sky plane is about $\sim\pi/2$ i.e. $\gamma\sim 0$ and $\beta\sim\pi/2$, the rotation of binary axis is so small. In that case, the orbital motion signature in the astrometric trajectories is ignorable especially when there is no caustic-crossing feature.

Depending on the size of the angular Einstein radius this effect can be seen in the astrometric trajectory. If there is no caustic-

crossing feature, the probability of detecting the photometric signature of orbital motion is so small.

3 MONTE CARLO SIMULATION

In this section we perform a Monte Carlo simulation to obtain quantitatively detectability of lens orbital motion in astrometric and photometric microlensing with rotating stellar-mass black holes. In the first step, we produce an ensemble of binary microlensing events with stellar-mass black holes as microlenses according to the physical distribution of parameters. Then, corresponding light curves and astrometric trajectories are generated according to the real data points from an ensemble of observatories in the microlensing experiment. By considering a detectability criterion, we investigate whether the signatures of lens orbital motion can be seen in observations of microlensing light curves and astrometric trajectories. Our criterion for detectability of orbital motion is $\Delta\chi^2 = \chi^2_{OM} - \chi^2_{SB} > \Delta\chi^2_{th}$ where χ^2_{OM} and χ^2_{SB} are the χ^2s of the known rotating binary microlensing model and the static model with the same binary parameters respectively. We assume that from fitting process and searching all parameter space the best-fitted solution is the known binary solution. Our aim is to compare photometric efficiency of detecting lens orbital motion with the astrometric one. Hence, we calculate $\Delta\chi^2$ for simulated light curves and astrometric trajectories independently.

Here, we explain distribution functions of the lens and source parameters. For lens parameters we take the mass of the stellar-mass black hole as the primary from the following distribution function (Farr et al. 2011):

$$P(M_l) \propto \exp(-\frac{M_l}{M_o}), \tag{12}$$

where $P(M_l) = dN/dM_l$ and $M_o = 4.7M_\odot$ in the range of $M_l \in [4.5, 25]M_\odot$. The mass ratio of the secondary to the primary is drawn from the distribution function (Duquennoy & Mayor 1991):

$$\rho(q) \propto \exp(-\frac{(q-q_0)^2}{2\sigma_q^2}) \tag{13}$$

where $\rho(q) = dN/dq$ in the range of $q \in [0.01, 1]$, $q_0 = 0.23$ and $\sigma_q = 0.42$. We choose the semi-major axis s of the binary orbit from the Öpik law where the distribution function for the primary-secondary distance is proportional to $\rho(s) = dN/ds \propto s^{-1}$ (Öpik 1924) in the range of $s \in [0.6, 30]Au$. The location of lenses from the observer is calculated from the probability function of microlensing detection $d\Gamma/dx \propto \rho(x)\sqrt{x(1-x)}$, where $x = D_l/D_s$ changes in the range of $x \in [0, 1]$ and $\rho(x)$ is the stellar density of thin disk, chosen from Rahal et al. (2009). The time of arriving at the perihelion point of orbit t_p is chosen uniformly in the range of $t_p \in [t_0 - P, t_0 + P]$. The projection angles to indicate the orientation of orbit of lenses with respect to the sky plane, i.e. β and γ, are taken uniformly in the range of $[-\frac{\pi}{2}, \frac{\pi}{2}]$. We take the eccentricity of the lenses' orbit uniformly in the range of $\varepsilon \in [0, 0.15]$.

For the source, we take the coordinate toward the Galactic bulge (l, b), distribution of the matter in standard Galactic model and generate the distribution of the source stars according to the Besancon model (Dwek et al. 1995; Robin et al. 2003). We assign the the absolute, apparent color and magnitude of the source star in the same approach which is explained in (Sajadian et al. 2013). The mass of source star is taken from the Kroupa mass function, $\xi = dN/dm \propto m_\star^{-\alpha}$, in the range of $m_\star \in [0.3, 3]M_\odot$, where

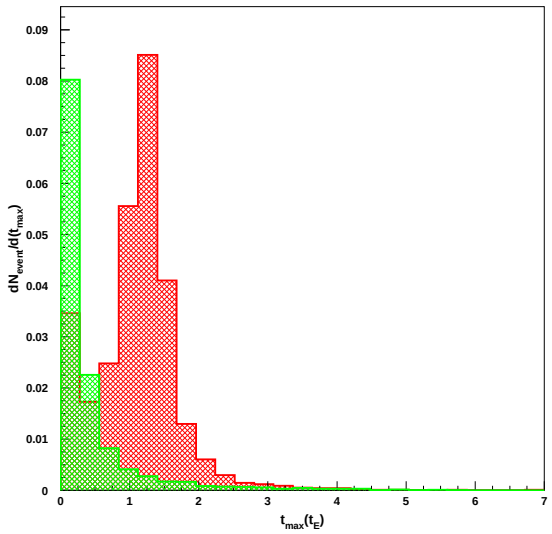

Figure 5. Distribution functions of the time, with respect to the time of the closest approach and in the unit of the Einstein crossing time, of the maximum photometric (green histogram) and astrometric (red histogram) deviations due to lens orbital motion for binary microlensing events with detectable effects of lens orbital motion in their light curves and astrometric trajectories respectively.

$m_\star$ is the mass of the source star in the unit of the solar mass and $\alpha = 0.3$ for $0.01 \leqslant m_\star \leqslant 0.08$, $\alpha = 1.3$ for $0.08 \leqslant m_\star \leqslant 0.5$ and $\alpha = 2.35$ for $m_\star \geqslant 0.5$ (Kroupa et al. 1993; Kroupa 2001). Another parameter we need in our simulation is the radius of source star. This parameter will be used in generating the light curve of microlensing events with the finite size effect. For the main-sequence stars, the relation between the mass and radius is given by $R_\star = m_\star^{0.8}$ where all parameters normalized to the sun's value. We did not consider giant source stars. For indicating the trajectory of the source with respect to the binary lens, we identify this path with an impact parameter and orientation defined by an angle between the trajectory of source star and the binary axis. We let this angle change in the range of $[0, 2\pi]$. The impact parameter is taken uniformly in the range of $u_0 \in [0, 1]$ and the corresponding time for u_0 is set zero.

The velocities of the lens and the source star are taken from the combination of the global and dispersion velocities of the Galactic disk and bulge (Rahal et al. 2009; Binney & Tremaine 1987). The relative velocities of the source-lens is determined by projecting the velocity of the source star into the lens plane.

We ignore the microlensing events in which the minimum distance between two lenses and also minimum impact parameter are not one order of magnitude larger than the Schwarzschild radius of the primary lens. Because they do not obey Keplerian laws.

Now, we generate data points over the light curves and astrometric trajectories. We assume that microlensing events are observed with the HST, OGLE and MOA surveys. The time interval between data points and the photometric uncertainties for each data point taken by survey telescopes are drawn from the archive of the microlensing light curves. The HST start observing these events after that the light curve reaches to a given threshold of magnification (i.e. $\frac{3}{\sqrt{5}}$). We suppose that the HST is monitoring these microlensing events with cadence one day. The other factor in simulation of

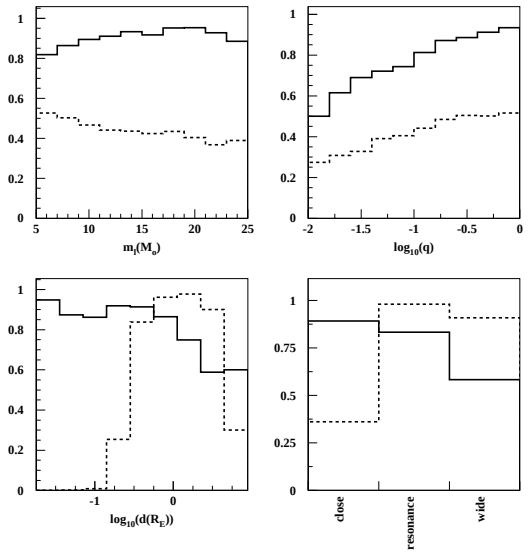

Figure 6. The astrometric (solid line) and photometric (dashed line) efficiencies of detecting lens orbital motion for different parameters of lenses and different topology of caustics (the last panel).

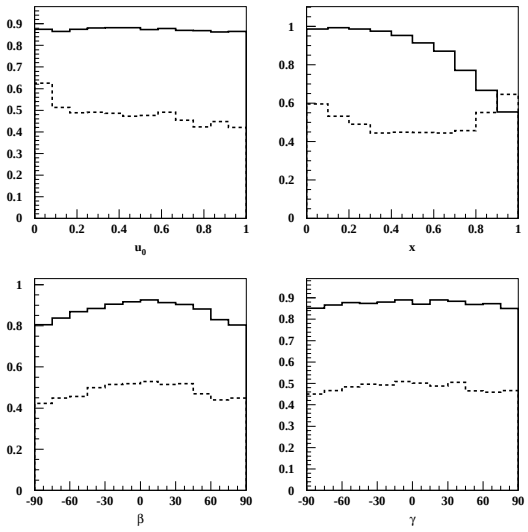

Figure 7. The astrometric (solid line) and photometric (dashed line) efficiencies of detecting lens orbital motion for different parameters of source star and lenses trajectories.

the light curve is the exposure time for each data point taken by the HST. From the exposure time we can calculate the the error bar for each data point. We can tune the exposure time in such a way that we have uniform error bars thought out the light curve. Here, we demand the photometric accuracy for each data point taken by the HST about 0.4 per cent which is chosen according to the recorded exposure times for those long-duration microlensing events being observed by the HST.

Astrometric observations of source star position are done by the HST with the astrometric accuracy of $\sigma_{as} = 200$ micro-arcsecond. The simulated astrometric data points are shifted according to the astrometric accuracy of the HST by a Gaussian function. A sample of the simulated light curve and astrometric trajectory of source star is shown in Figure (4). In this figure the data taken by survey telescopes and the HST are shown with violet points and black stars. The parameters used to make this event are brought in the fourth row of table (2). The time-variation rate of the astrometric centroid shift vectors is not constant. As a result, in some places over the astrometric trajectory the HST data points do not uniformly set despite similar cadences (see Figure 4). In this event, the orbital motion effect is obvious in the astrometric trajectory as well as the photometric light curve.

Our criterion for detectability of orbital motion is $\Delta\chi^2 = \chi^2_{OM} - \chi^2_{SB} > \Delta\chi^2_{th}$. We consider $\Delta\chi^2_{th} = 250$ for both photometric and astrometric observations. From the Monte Carlo simulation we obtain that 80.2, 16.9 and 2.9 per cent of total simulated events are close, intermediate and wide binaries and the average detection efficiency $< \epsilon_{OM} >$ for the orbital motion detection in the astrometric trajectories and the amplification light curves of binary microlensing events with stellar-mass black holes are 87.3 and 48.2 per cent, respectively. As a result, in these events lens orbital motion can be seen most likely in astrometric trajectories whereas photometric signatures of orbital motion are often too small to be detected. Detecting lens orbital motion in their astrometric trajectories helps to discover further secondary components around the primary lens as well as resolve close/wide degeneracy.

In Figure (5) we plot the distribution functions of the time of the maximum photometric (green histogram) and astrometric (red histogram) deviations due to lens orbital motion, measured with respect to the time of the closest approach and in the unit of the Einstein crossing time i.e. t_{max}, for binary microlensing events with detectable effects of lens orbital motion in their light curves and astrometric trajectories respectively. According to this figure, the orbital motion signature in the astrometric trajectory can be seen at sometime often after one Einstein crossing time with respect to the time of the closest approach whereas this signal in the light curve can be detected at sometime almost before it. In wide or intermediate binary events with detectable astrometric signatures of orbital motion, the maximum deviation happens at very late time, e.g. $t - t_0 \geqslant 6t_E$, which have made some so small peaks in Figure (5).

In order to study the sensitivity of detecting orbital motion in astrometric trajectories of source star and photometric light curves on the parameters of the model, we plot the astrometric (solid line) and photometric (dashed line) detection efficiencies in terms of the relevant parameters of the binary lens and source in Figures (6) and (7). We ignore the irrelevant parameters that do not change the efficiency function. The detection efficiency function in terms of the binary lens and source parameters is given as follows.

(i) The first parameter is the primary lens mass, M_l. Here, the astrometric efficiency of detecting lens orbital motion rises with increasing the primary lens mass. The physical interpretation of this feature is that the angular Einstein radius and as a result of it the astrometric signal rise with increasing the primary lens mass. On the photometric detection efficiency there are two factors that effect inversely. With increasing the primary lens mass the Einstein radius rises which decreases the normalized distance between two lens components and the caustic size. On the other hand, the ratio of the Einstein crossing time to the orbital period of lenses motion

increases. However, the first effect is dominant. Because, the photometric signature of orbital motion can more likely be detected while the source is crossing the caustic.

(ii) The second parameter is the ratio of the lens masses, q. The ratio of the lens masses has a geometrical effect on the shape of the caustic lines, where increasing it towards the symmetric shape maximizes the detection efficiency. Indeed, the size of the central caustic scales as q (Gaudi 2012).

(iii) The third parameter is the projected Semi-major axis of lens orbit normalized to the Einstein radius. The photometric detection efficiency has the maximum amount around $1R_E$ in which the caustic curves have the maximum size. However, the astrometric detection efficiency has the highest amount for close binaries with the large ratio of the Einstein crossing time to the orbital period.

(iv) Different topologies of caustic curve: The astrometric and photometric detection efficiencies are maximized in close and intermediate binaries respectively. Indeed, the size of the central caustic which indicates the probability of caustic crossing and the detectability of lens orbital motion photometrically has the highest amount for the intermediate microlensing events (see Figure 1). Note that most simulated events are close binaries.

(v) Impact parameter, u_0, shown in Figure (7): Decreasing the impact parameter increases the photometric detection efficiency. A smaller impact parameter from the center of the lens configuration rises the probability of the caustic crossing. However, the astrometric detection efficiency does not depend on the impact parameter.

(vi) The next parameter is $x = D_l/D_s$ the relative distance of the lens to the source star from the observer. The angular Einstein radius and astrometric signals increase by decreasing x. On the other hand, the Einstein radius has the highest amount around $x = 0.5$. When x tends to 0.5, by increasing the Einstein radius the normalized distance between two lens components and the probability of the caustic crossing decrease.

(vii) and (viii) Inclination angles of orbital plane of lenses with respect to the sky plane, β and γ. The astrometric detection efficiency is maximized in $\beta \sim 0$ and $\gamma \sim \pm\pi/2$ in which the rotation angle of the source trajectory with respect to the binary axis owing to lens orbital motion, θ_l, has the maximum amount.

4 CONCLUSIONS

In this work we investigated lens orbital motion in astrometric microlensing and its detectability. In microlensing events, the astrometric centroid shift in source trajectories falls off much more slowly than the light amplification as the source distance from the lens position increases. Hence, perturbations developed with time e.g. the effect of lens orbital motion make considerable deviations in astrometric trajectories whereas the photometric signal of orbital motion can mostly be detected when the source is around the caustic curve.

The orbital motion of lenses changes the magnification pattern by changing the projected distance between two lenses as well as rotates the straightforward source star trajectory with respect to the binary axis. These effects can be seen in the microlensing light curve if lenses rotate each other considerably when the source star is around the caustic curve. At the same time, the orbital motion of lenses rotates the astrometric trajectory in the same was as the source trajectory. Depending on the size of the angular Einstein radius this effect can be seen at sometime often after one Einstein crossing time with respect to the time of the closest approach while this signal in the light curve can be detected at sometime almost before it.

Binary microlensing events with rotating stellar-mass black holes which have detectable astrometric shifts in the source star trajectories have most likely detectable orbital motion signatures. In these events, the ratio of the Einstein crossing time to the orbital period is high. Although, orbital motion effect in their light curves is too small especially when there is no caustic-crossing feature, but the astrometric signature owing to the orbital motion can be detected at the end parts of astrometric trajectories. In addition, the Hubble Space Telescope (HST) is observing some long-duration microlensing events which are likely to be owing to stellar-mass black holes, following the approved proposal by Sahu et al. (2010). Hence, we expect that if there is a secondary lens, the astrometric signature of its orbital motion can much probably be observed.

By performing Monte Carlo simulation we evaluated the efficiency of detecting orbital motion in astrometric and photometric microlensing with binary stellar-mass black holes. We considered $\Delta\chi^2 > 250$ as the detectability criterion and concluded that astrometric efficiency is 87.3 per cent whereas the photometric efficiency is 48.2 per cent. From total simulated events 80.2, 16.9 and 2.9 per cent were close, intermediate and wide binaries respectively. Also, the more massive lenses, the more detectable signatures of orbital motion. Detecting orbital motion in binary microlensing events helps not only to detect further secondary components even without any photometric binarity signature but also to resolve close-wide degeneracy as well.

Acknowledgment I am especially thankful to Sohrab Rahvar for his encouragement, useful discussions and reading of the manuscript. I would like to thank Martin Dominik for generalizing his adaptive contouring algorithm to calculate the astrometric shifts in binary microlensing events, Matthew Penny for pointing out an important error, Andy Gould and Cheongho Han for careful reading and commenting on the manuscript. Finally, I thank the referee for useful comments and suggestions which certainly improved the manuscript.

REFERENCES

An J. H., et al., 2002, ApJ, 572, L521.
Binney, S., & Tremaine, S. 1987, Galactic Dynamics. Princeton Univ. Press, Princeton, NJ.
Chang K., Refsdal S., 1979, Nature, 282, L561.
Chung S.-J., Park B.-G., Ryu Y.-H. & Humphrey A. 2009, APJ, 695, L1357.
Dominik M., 2007, MNRAS, 377, L1679.
Dominik M. & Sahu K. C., 2000, ApJ., 534, L213.
Dominik M. 1999, A & A, 349, L108.
Dominik M., 1998, A & A, 329, L361.
Dong S., Gould A., Udalski A., et al., 2009, ApJ, 695, L970.
Duquennoy A. & Mayor M., 1991, A & A, 248, L485.
Dwek, E., Arendt, R. G., Hauser, M. G., et al., 1995, ApJ, 445, L716.
Einstein A., 1936, Science, 84, L506.
Farr W. M., Sravan N., Cantrell A., Kreidberg L., Bailyn C. D., Mandel I. & Kalogera V., 2011, ApJ, 741, L103.
Gaudi B. S., et al., 2008, Sci, 319, L927.
Gaudi B. S., 2012, Annu. Rev. Astron. Astrophys., 50, L411.
Gould A. & Han C. 2000, ApJ, 538, L653.
Gould A., Shin I. -G., Han C., Udalski A. & Yee J. C., 2013, ApJ, 768, L126.

Han C.,Chun M.-S. & Chang K. 1999, ApJ, 526, L405.
Høg, E., Novikov, I. D., & Polnarev, A. G. 1995, A & A , 294, L287.
Ioka K., Nishi R. & Kan-Ya Y., Prog. Theor. Phys., 102, L983.
Jeong Y., Han C. & Park S.-H. 1999, ApJ,511, L569.
Kroupa, P., Tout, C. A., & Gilmore, G. 1993, MNRAS, 262, L545.
Kroupa, P. 2001, MNRAS, 322, L231.
Liebes, Jr.S., 1964, Phys. Rev., 133, L835.
Miralda-Escudé J., 1996, ApJ, 470, L113.
Miyamoto, M. & Yoshii, Y. 1995, AJ, 110, L1427.
Öpik, E., 1924, Pulications de. L'Observatoire Astronomique de l'Université de Tartu, 25, L6.
Paczyński B., 1986a, ApJ, 301, L502.
Paczyński B., 1986b, ApJ, 304, L1.
Paczyński B., 1995, Acta Astron., 45, L345.
Paczyński B., 1997, Astrophys. J. Lett. astro-ph/9708155.
Penny M. T., Mao S. & Kerins E., 2011, MNRAS, 412, L607.
Proft A., Demleitner M. & Wambsganss J., 2011, A & A, 536, L50.
Rahal, Y. R., Afonso C., Albert J.-N., et al. 2009, A & A, 500, L1027.
Rattenbury N. J., Bond I. A., Skuljan J. & Yock P. C. M., 2002, MNRAS, 335, L159.
Robin, A. C., Reylé, C., Derrière, S., Picaud, S., 2003, A & A, 409, L523.
Sajadian, S., Rahvar, S. & Dominik M., 2013, in preperation.
Sahu K. C., Bond H. E., Anderson J., Udalski A., Dominik M. & Yock P., 2010, the proposal number: 13458.
Sahu K. C., 2011, Oral Presentation at 15th Microlensing Workshop, Salerno.
Sahu K. C., 2011, Oral Presentation at annual MindStep meeting, Qatar.
Shin I. -G., Udalski A., Han C. et al. 2011, ApJ, 735, L85.
Shin I. -G., Han C., Choi J. -Y., et al. 2012, ApJ, 755, L91.
Shin I. -G., Sumi T., Udalski A., et al., 2013, ApJ, 764, L64.
Walker M. A. 1995, ApJ, 453, L37.